Penerbit Akademia Baru

Journal of Advanced Research in Fluid Mechanics and Thermal Sciences

Journal homepage: www.akademiabaru.com/arfmts.html
ISSN: 2289-7879

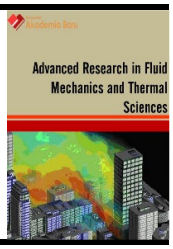

Numerical Study For Flow Over A Realistic Generic Model, DrivAer, Using URANS

Open Access

Nur Haziqah Shaharuddin[1], Mohamed Sukri Mat Ali[1,*], Shuhaimi Mansor[2], Sallehuddin Muhamad[3], Sheikh Ahmad Zaki[1]

[1] Wind Engineering for Environment, Malaysia-Japan International Institute of Technology, Universiti Teknologi Malaysia, 54100 Kuala Lumpur, Malaysia
[2] Faculty of Mechanical Engineering, Universiti Teknologi Malaysia, 81310 Skudai, Johor, Malaysia
[3] Razak School of Engineering and Advanced Technology, Universiti Teknologi Malaysia, 54100 Kuala Lumpur, Malaysia

ARTICLE INFO

Article history:
Received 14 February 2018
Received in revised form 16 May 2018
Accepted 10 August 2018
Available online 16 August 2018

ABSTRACT

The aim of this study is to present a systematic approach for the grid convergence analysis in simulating flow around a realistic generic model, DrivAer. The numerical simulation is modelled using unsteady Reynolds Averaged Navier-Stokes (URANS) equation. A minimum of three different grid resolutions are considered, which are fine, medium and coarse in order to investigate the grid independency. Richardson extrapolation and Grid Convergence Index (GCI) are introduced to quantitatively evaluate the grid independency. Based on the results between those three different grids, a monotonic convergence criteria has been achieved. The reduction in GCI value indicates that the grid convergence error has been significantly reduced, in which the fine grid has a GCI value less than 7%. Additionally, the result from the fine grid is only 6% difference if compared with previous experimental study.

Keywords:
CFD, DrivAer, Grid Convergence Index, OpenFOAM simulation, URANS

1. Introduction

Since 2011, study of flow around a realistic generic vehicle model, DrivAer, has been continuously be the subject of many research [1-5]. DrivAer is a generic vehicle model proposed by the Technical University of Munchen (TUM), in cooperation with Audi AG and BMW Group. The model has been designed closely similar as the production car. Recently, most of the automotive aerodynamic research usually relied on simplified car models such as the Ahmed Body [6] and the SAE Type 4 (fullback) model [16]. These simplified car models could represent data for a basic understanding flow structures. However, the simplified models are unable to produce a detailed flow phenomena similar to a real production car. Shaharuddin *et al.,* [7] has compared the aerodynamic and flow pattern between the SAE Type 4 (fullback) model and DrivAer Fastback model and confirm that the simplified car model (SAE Type 4) is unable to represent the detailed flow structures but for the

* *Corresponding author.*
E-mail address: sukri.kl@utm.my (Mohamed Sukri Mat Ali)

DrivAer model, the flow structures are more complex and very similar to a real production car. The DrivAer is introduced by TUM to represent the actual flow behaviour around the car. A study conducted by Heft *et al.,* [1] has shown that most of the complex flow structures occurred around a real production car can be correctly captured by using the DrivAer model, whereas the simplified car models produced a simple flow structures.

Despite the fact that there are many similar investigations have been made numerically by using the DrivAer model, there is still a small variation shown by the results obtained. This could be due to the differences in the construction and distribution of the mesh. Four different meshes have been used by Guilmineau [2] in order to investigate the flow around a DrivAer fastback model by using the Explicit Algebraic Reynolds Stress Model (EARSM) turbulence model. The coarsest mesh is 19 million cells and the finest mesh is 45 million cells. Results shown that all meshes under-predict the drag coefficient compared to the experimental data. This shows that the used of high number of mesh excessively is not a guarantee to provide a similar result as the experimental data. Additionally, it requires high computational cost and it is impractical for the industry. Therefore, in order to verify that the results obtained are acceptable and reliable, for any numerical study, it is important to investigate the sensitivity of each grid resolution on certain flow properties in a systematic manner.

Computational Fluid Dynamic (CFD) community agree that the source of errors from the numerical simulation is not entirely due to the grid convergence error, but also affected by the other factors. However, the total error can be minimised by reducing the error due to the grid dependency and this should be done systematically. Therefore, the purpose of this study is to present a systematic approach for grid convergence on the simulation of flow around a realistic generic model, DrivAer, by using Grid Convergence Index (GCI) that is based on the Richardson extrapolation.

2. Methodology

2.1 Model Description

The model used in this study is an open-source realistic generic vehicle model, DrivAer, which has a similar exterior design and dimension as the existing passenger cars. Thus, it would provide more realistic results. The detailed geometry of the model is shown in Figure 1. It is a fastback model with a smooth underbody.

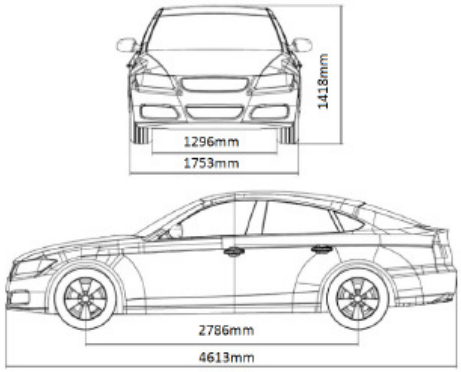

Fig. 1. Baseline configurations in current study, DrivAer Fastback [8]

The length (L), height (H) and width (W) of the DrivAer Fastback geometry are 4613mm, 1418mm and 1753mm, respectively.

2.2 Computational Domain

The size of the numerical wind tunnel (computational domain) is $10\mathrm{L} \times 8\mathrm{H} \times 5.5\mathrm{W}$. The distance from the inlet to the model is 2L. Meanwhile, the distance from the model to the outlet is made large, which is 7L for allowing the wake to dissipate naturally. The model is made attached to non-moving ground. In order to reduce the computational time, only half of the model is simulated. Figure 2 and 3 show the schematic diagram of the computational domain.

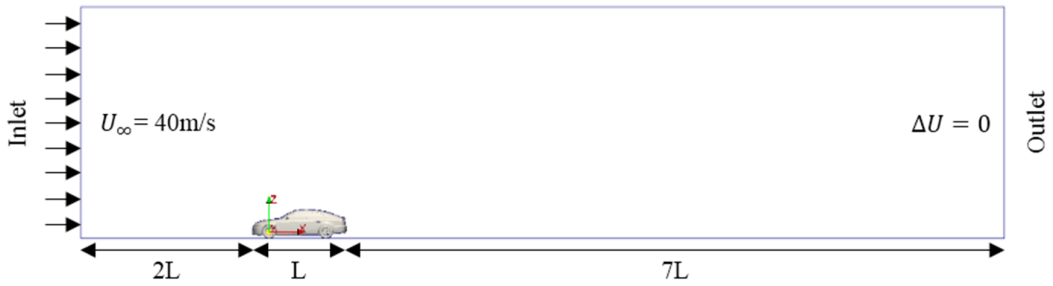

Fig 2. Side view

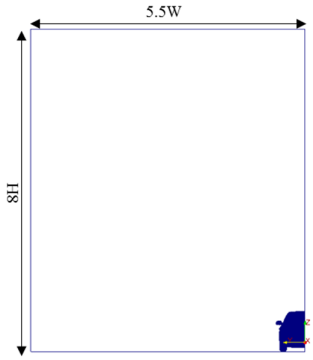

Fig 3. Front view

Free stream velocity (U_∞) in the x-direction is fixed for the inlet condition to drive wind flow through the internal domain. At the upstream floor, slip boundary condition is imposed to prevent the development of boundary layer, while no slip boundary condition is imposed at the downstream to allow the effect of viscosity from the wake interacts with the downstream floor.

2.3 Mesh Description

The mesh inside the computational domain is constructed by using the mesh generation utility, *blockMesh*, which is a primary meshing tool provided in the OpenFOAM software, while the mesh refinement around the DrivAer model is generated by using another mesh generation utility that is also supplied with the OpenFOAM, which is *snappyHexMesh* that generates unstructured mesh. Based on the grid refinement factor (*r*), three different grid resolutions are considered in this study which is fine, medium and coarse grids. Celik *et al.,* [9] stated that, in order to optimise the accuracy of turbulent flow prediction, a desirable value of *r* has to be greater than 1.3. The grid refinement factor (*r*) can be calculated as follows;

$$r_{21} = \frac{h_2}{h_1} \tag{1}$$

$$r_{32} = \frac{h_3}{h_2} \quad (2)$$

where the subscripts 1,2 and 3 indicate the types of grid used which are fine, medium and coarse, respectively. Meanwhile *h* represents the average cell size, mesh or grid size. For three dimensional (3D), the average cell size can be calculated by using the following equation [9];

$$h_{ave} = [\frac{1}{N}\sum_{i=1}^{N}(\Delta v_i)]^{1/3} \quad (3)$$

where *N* is the total number of cells used for the computation and Δv_i is the volume of the *i*th cell. Table 1 shows the grid parameters for the three cases. The mesh generation and distribution for the fine case are shown in Figure 4.

Table 1
Parameters used for all cases

Case	Fine (1)	Medium (2)	Coarse (3)
Total No. of Cells, *N*	4 711 750	2 137 902	851 152
Average cell size, h_{ave}	0.1036	0.1348	0.1833
Refinement ratio, *r*	r_{21} = 1.30	r_{32} = 1.36	

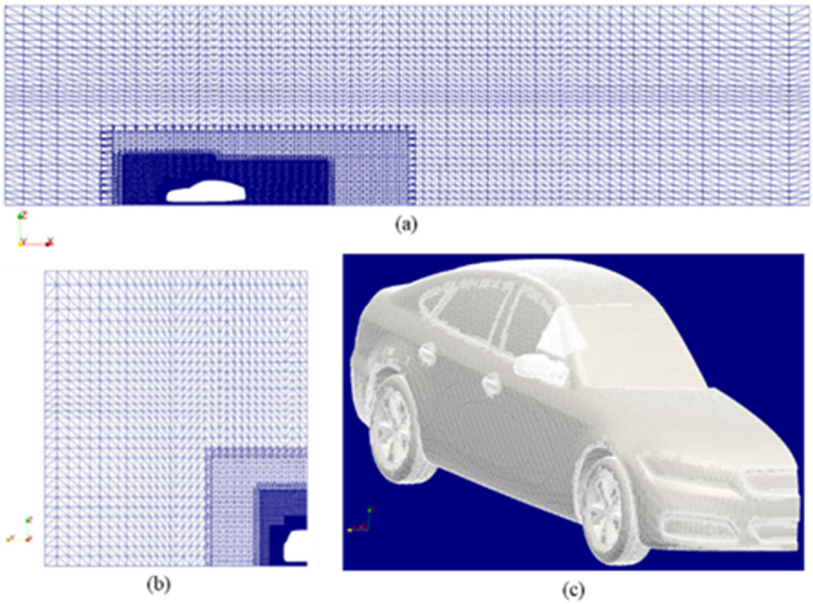

Fig. 4. Mesh generation for the fine case. (a) Mesh on the $x - z$ plane (b) Mesh on the $y - z$ plane (c) Mesh on the DrivAer Fastback model

2.4 Numerical Setting
2.4.1 Governing equation

The governing equations for the turbulent incompressible flow encountered in the current study are the unsteady Reynolds-Averaged Navier-Stokes (URANS) equations as follows.

Continuity

$$\rho \frac{\partial U_i}{\partial x_j} = 0 \quad (4)$$

Momentum

$$\rho \frac{\partial U_i}{\partial t} + \rho U_j \frac{\partial U_i}{\partial x_j} = \frac{\partial}{\partial x_j} \left[-\bar{p}\delta_{ij} + \mu \left(\frac{\partial U_i}{\partial x_j} + \frac{\partial U_j}{\partial x_i} \right) - \rho \overline{u_i' u_j'} \right] \quad (5)$$

where $\rho\overline{u_i'u_j'}$ is the Reynolds stress, which then is solved using eddy-viscosity model based on the Boussinesq assumption.

$$-\overline{\rho u_i{}' u_j{}'} = \mu_t \left(\frac{\partial \overline{u_i}}{\partial x_j} + \frac{\partial \overline{u_j}}{\partial x_i} \right) - \frac{2}{3} \left(\rho k + \mu_t \frac{\partial \overline{u_k}}{\partial x_k} \right) \delta_{ij} \quad (6)$$

where μ_t the turbulent or eddy viscosity and *k* is the turbulent kinetic energy.

2.4.2 Turbulence model

The turbulent kinetic energy (*k*) and the specific dissipation rate (ω) are solved using the two equations model that is based on Shear Stress Transport (SST) *k*-ω [10];

$$\frac{\partial k}{\partial t} + U_j \frac{\partial k}{\partial x_j} = P_k - \beta^* k\omega + \frac{\partial}{\partial x_j} \left[(v + \sigma_k v_T) \frac{\partial k}{\partial x_j} \right] \quad (7)$$

$$\frac{\partial \omega}{\partial t} + U_j \frac{\partial \omega}{\partial x_j} = \alpha S^2 - \beta \omega^2 + \frac{\partial}{\partial x_j} \left[(v + \sigma_\omega v_T) \frac{\partial \omega}{\partial x_j} \right] + 2(1 - F_1)\sigma_{\omega 2} \frac{1}{\omega} \frac{\partial k}{\partial x_i} \frac{\partial \omega}{\partial x_i} \quad (8)$$

where v_T is kinematic eddy viscosity and it is defined as;

$$v_T = \frac{a_1 k}{max(a_1 \omega, SF_2)} \quad (9)$$

2.4.3 Boundary condition

A uniform velocity, $U = 40m/s$, is imposed at the inlet as well as at the top and side of the computational domain as stated in Table 2. Based on the length (L) of the DrivAer Fastback model, the Reynolds number is, *Re = 4.87 x 10*^{6} which make the flow is fully turbulent. The flow is assumed incompressible as the Mach number is below than 0.3.

Table 2
Numerical boundary conditions for DrivAer model

	Inlet	Outlet	Top	Side	Downstream & DrivAer Fastback	Upstream
$k\ (m^2 s^2)$	fixedValue (0.0016)	zeroGradient	fixedValue (0.0016)	fixedValue (0.0016)	kqRWallFunction	slip
$\omega\ (s^{-1})$	fixedValue (4.36)	zeroGradient	fixedValue (4.36)	fixedValue (4.36)	omegaWallFunction	slip
$nut\ (m^2/s)$	fixedValue (3.69×10^{-4})	zeroGradient	fixedValue (3.69×10^{-4})	fixedValue (3.69×10^{-4})	nutkWallFunction	slip
$p\ (kg/ms^2)$	zeroGradient	0	zeroGradient	zeroGradient	0	slip
$U\ (m/s)$	fixedValue (40)	zeroGradient	fixedValue (40)	fixedValue (40)	zeroGradient	slip

Some important settings used in the OpenFOAM software are shown in Table 3. The discretization schemes used are at least in the second-order accuracy and this has been applied to all equations.

Table 3
Solver settings used in OpenFOAM

Discretization	Scheme
Temporal discretization	Backward (2nd order implicit)
Gradient	Central differencing (2nd order)
Divergence	QUICKV (3rd order)
Laplacian	Gauss linear differencing scheme (2nd order unbounded)
Pressure-velocity Coupling	PIMPLE
Turbulence model	URANS SST *k-ω*

Table 4 shows three different time step used based on the different grid cases in order to ensure that the Courant-Fredichs-Lewy (CFL) number always below 0.8.

Table 4
Time step for all cases

Case	Fine (1)	Medium (2)	Coarse (3)
Time step (Δt)	0.000005	0.000025	0.00003

3. Results and Discussions

3.1 Richardson Extrapolation

Richardson extrapolation [11] is used to calculate a higher-order estimate of the continuum value (value at zero grid spacing) from a series of lower-order discrete values. In grid refinement study, the value estimated from the Richardson extrapolation is obtained if the cell grid size tends to zero ($h \rightarrow 0$). Extrapolation is made at least from the comparison between two different grid resolutions results. Nevertheless, Stern *et al.,* [17] stated that a minimum of three grid resolutions are required for a convergence study.

The Richardson extrapolation can be generalised by p^{th} – order methods [12];

$$f_{RE} \approx f_1 + \left[\frac{(f_1 - f_2)}{(r^p - 1)}\right] \tag{10}$$

where *r* is the grid refinement ratio as mentioned in (1) and (2).

From (10), the extrapolated value is varied due to different order of accuracy (p) that can be estimated as follows;

$$p = \frac{1}{ln(r)}\left|ln\left|{}^{\varepsilon_{32}}/_{\varepsilon_{21}}\right| + q(p)\right| \tag{11}$$

$$\varepsilon_{32} = f_3 - f_2 \tag{12}$$

$$\varepsilon_{21} = f_2 - f_1 \tag{13}$$

$$q(p) = ln\left(\frac{r_{21}^p - s}{r_{32}^p - s}\right) \tag{14}$$

$$s = 1.sign\left(\varepsilon_{32}/\varepsilon_{21}\right) \quad (15)$$

Note that $q(p) = 0$ if the grid refinement ratio is constant (i.e., $r_{21} = r_{32}$). However, the grid refinement ratio in the current study is not constant ($r_{21} \neq r_{32}$) as shown in Table 1 and therefore the extrapolated value differs based on the order of accuracy (p).

In order to evaluate the extrapolated value of these resolutions, the convergence condition must be first determined, where there are three possible convergence conditions;

1. Monotonic convergence ($0 < R < 1$)
2. Oscillatory convergence ($R < 0$)
3. Divergence ($R > 1$)

where R is the convergence ratio that is defined as follows;

$$R = \frac{\varepsilon_{21}}{\varepsilon_{32}} \quad (16)$$

3.2 Grid Convergence Index

Grid Convergence Index (GCI) provides a uniform manner in reporting the results of grid convergence studies [12] in which it will gives a result that approaches the actual result as the grid size approaches to zero. It is based on the estimated fractional error derived from the generalised Richardson Extrapolation. GCI represents the percentage of the computed value that is away from the value of the asymptotic numerical value and how much the resolution would be affected with a further grid refinement. A small value of GCI shows that the computation is within the asymptotic range. There have been many published studies that showing the GCI results for many fundamental and engineering problems [9], [12-15]. However, there is still no reported study on the GCI for a numerical simulation of a realistic car model. The GCI result is important as it can be the benchmark for future numerical study.

The GCI for the fine grid resolution is calculated as follows;

$$GCI_{i+1,i} = F_s \frac{|\varepsilon_{i+1,i}|}{f_i(r^p - 1)} \times 100\% \quad (17)$$

where F_s is the safety factor. According to Wilcox [18], for comparisons between three or more grids, the safety factor considered is 1.25.

The percentage error between the simulation value and the extrapolated value based on Richardson extrapolation is calculated as follows;

$$E_i = \left|\frac{f_i - f_{RE}}{f_{RE}}\right| \times 100\% \quad (18)$$

For a better analysis, it is suggested to consider three levels of grid resolution in order to correctly evaluate the order of convergence and to ensure that the solutions are within the asymptotic range of convergence. Studies on grid refinement by Ali *et al.,* [13], Ishak *et al.,* [14] and Maruai *et al.,* [15] have also considered three level of grid resolutions in which their results show that the grid refinement is achieving a monotonic converged criteria that indicates the grid convergence error is progressively reduced.

Table 5
Comparison of forces coefficient parameter between the three mesh resolutions and the extrapolated value based on Richardson Extrapolation calculation

Case	Fine (f_1)	Medium (f_2)	Coarse (f_3)	f_{RE}
Drag Coefficient, C_{Dmean}	0.2456	0.2524	0.2652	0.2333
f_i/f_{RE}	1.0527	1.0819	1.1367	
Error (%)	5.2718	8.1865	13.6730	
Lift Coefficient, C_{Lmean}	-0.0510	-0.0490	-0.0436	-0.0539
f_i/f_{RE}	0.9462	0.9091	0.8089	
Error (%)	5.3518	9.0635	19.0851	

The results of forces coefficient parameter obtained from the simulation of the three grid resolutions and its corresponding extrapolated values based on Richardson Extrapolation equation are represented in Table 5. Two parameters are considered which are, the mean drag and mean lift coefficients. Both forces coefficient are calculated once a statistically steady data is obtained. Percentage error for the three grid resolutions also are calculated using Equation (18) in which the fine mesh gives the percentage of error below 6%.

Table 6
Order of accuracy and Grid Convergence Index for three grid resolution based on forces coefficient parameter

Case	$\lvert\varepsilon_{32}\rvert$	$\lvert\varepsilon_{21}\rvert$	R	p	$GCI_{32}(\%)$	$GCI_{21}(\%)$
C_{Dmean}	0.0132	0.0070	0.5313	1.6708	9.4588	6.2598
C_{Lmean}	0.0054	0.0020	-0.0539	2	16.2486	7.0680

Table 6 summarises the order of accuracy and Grid Convergence Index (GCI) values. The convergence ratio for both parameter, drag and lift, shows that the refinement condition is monotonic as the value is in the range of $0 < R < 1$. The GCI value between fine and medium grid is relatively small compared to the GCI value between medium and coarse grid. This indicates that the dependency of the numerical simulation on the cell size has been reduced and the fine grid is nearly grid independent. In addition, further refinement of the fine grid resolution will not give a great impact on the simulation results.

The comparison between the mean drag coefficient C_{Dmean} and the Richardson extrapolation value for all three grids are shown in Figure 5. The discrepancy between the resolution and the extrapolated value becomes smaller as the grid is refined. The ratio between the result obtained using the fine grid with the estimated value using the Richardson extrapolation is $f_1/f_{RE} = 1.0527$. This corresponds to a minimum error of $E_1 = 5.2718\%$ as compared to the extrapolated value. Percentage errors between the three different grid resolutions are shown in Figure 6. The error values also have shown a reduction when approaching the fine grid.

From the calculation between the GCI and extrapolated value for fine grid, for an applicable and reliable grid or mesh, the maximum and minimum values for the extrapolated values are 1.1186 and 0.9868, respectively.

Result from mean lift coefficient C_{Lmean} also has shown that there is a reduction in the GCI value for fine grid when compared with coarse order grid resolution ($GCI_{21} < GCI_{32}$). According to the GCI value of fine grid and based on ratio between the fine grid and the extrapolated value, its maximum and minimum values are 1.0131 and 0.8793, respectively as shown in Figure 7. The percentage error also is decreased when the grid becomes finer as observed in Figure 8 where the error for fine grid is 5.3518%.

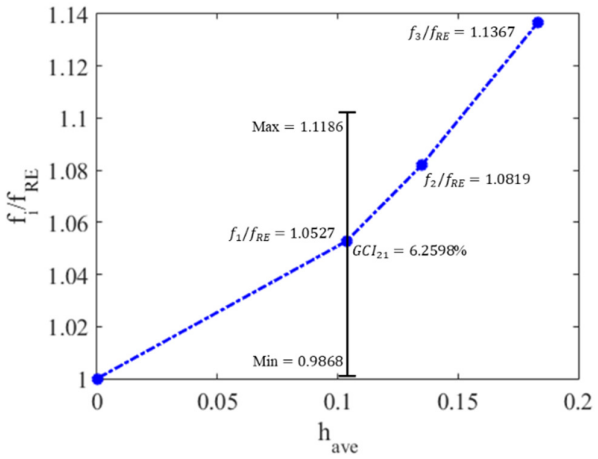

Fig. 5. Extrapolated value of C_{Dmean}

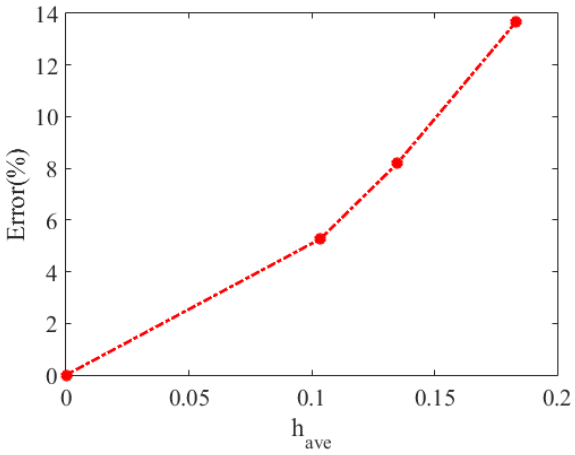

Fig. 6. Percentage error for C_{Dmean}

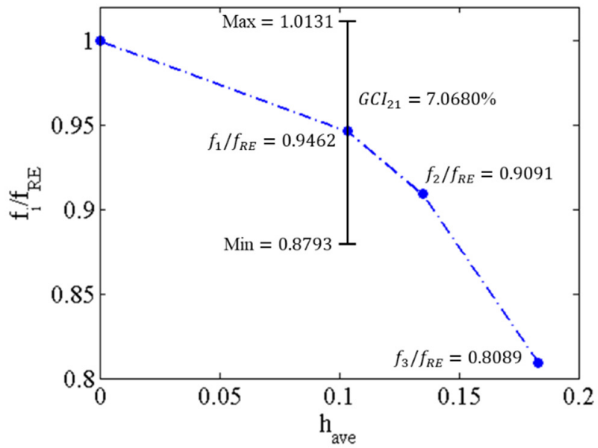

Fig. 7. Extrapolated value of C_{Lmean}

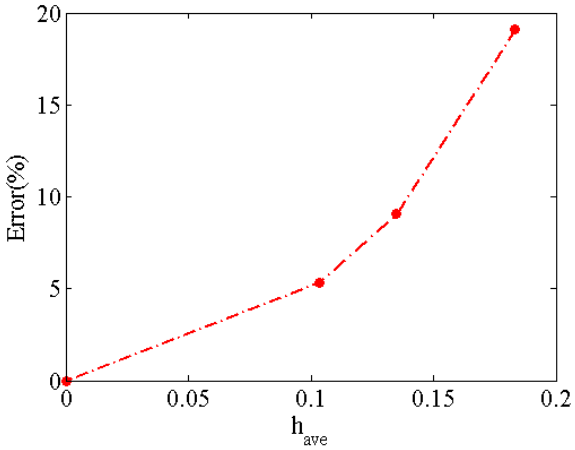

Fig. 8. Percentage error for C_{Lmean}

3.3 Forces Coefficient and Flow Visualisation

In order to reduce the computational cost, the cell size near the surface is properly treated by using the wall function. The overall number of grids can be minimized, especially at the near-wall regions while maintaining the accuracy of the computational result [14]. The corresponding average y^+ values on the DrivAer Fastback body and ground floor (downstream) for all cases are shown in Table 7. On the body, the y^+ values are on the log-law region which is in the range of $30 < y^+ < 300$. Meanwhile a greater y^+ is generated at the ground floor, but the values are still accepted since the main focused is given on the mesh generation around the model. Generally, fine grid case has shown a lower y^+ values compared to the other two cases and its distribution of y^+ on the body can be observed in Figure 9.

Table 8 compares the drag coefficient (C_D) results of current study for the fine grid case with previous available data. It shows that the results obtained in the current study for the unsteady case has a good agreement with the experimental results provided by Guilmineau [2] and Heft *et al.,* [1]. Overall, current results obtained are below 6% difference compared to the previous studies.

Table 7
The y^+ values on the wall for all cases

Case	Body			Ground Floor		
	y^+min	y^+max	y^+avg	y^+min	y^+max	y^+avg
Fine (f_1)	0.5412	675.2739	54.7379	1.0030	8085.6739	428.8274
Medium (f_2)	0.7472	566.4583	112.8169	4.5087	9076.7770	702.3972
Coarse (f_3)	1.3404	974.7539	153.9980	0.1786	7722.4127	738.3401

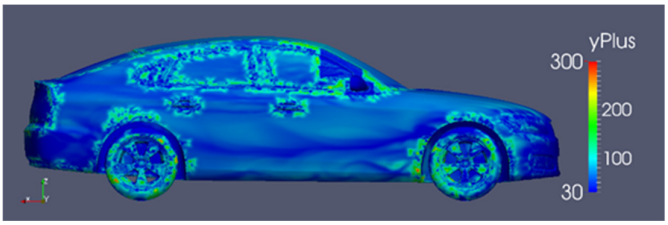

Fig. 9. Distribution of y^+(yPlus) on the DrivAer Fastback model

Table 8
Comparison of drag coefficient (C_D) between current study and previous studies

Turbulence Model	Method	Drag Coefficient (C_D)	%Δ
Current (Fine)	*k-ω* SST (Steady)	0.2542	2.61%
Current (Fine)	*k-ω* SST (Unsteady)	0.2456	5.90%
Heft *et al.,* [1]	*k-ω* SST (Steady)	0.2410	7.66%
Guilmineau [2]	RANS (EARSM) (Steady)	0.2573	1.42%
Shinde *et al.,* [3]	*k-ω* SST (Steady)	0.2510	3.83%
Ashton *et al.,* [4]	*k-ω* SST (Steady)	0.2600	0.38%
Ashton *et al.,* [4]	Realisable k-ε (RKE) (Steady)	0.2440	6.51%
Heft *et al.,* [1]	Experiment	0.2430	6.90%
Guilmineau [2]	Experiment	0.2610	-

Result from the URANS numerical simulation for the vortex structure around the DrivAer Fastback model using the iso-surface of the second invariant of velocity gradient (Q) is shown in Figure 10. Compared to the current study that used only 4.7 million cells, the flow characteristics captured a similar flow pattern as the study done by Guilmineau [2] which has been done with a total of 45 million number of cells using RANS approach. Note that different contours are used between both figures. However similar pattern of A-pillar vortex is observed in both figures, in which a conical shape that elevated downstream is formed. Moreover, it is clearly can be observed that the flow is detached at the side view mirror and at the A-pillar. A long conical wake is produced near the side view mirror and also there are vortex structures generated by the wheels and at the rear end of the model. Similar flow structures are also observed by Aljure *et al.,* [5].

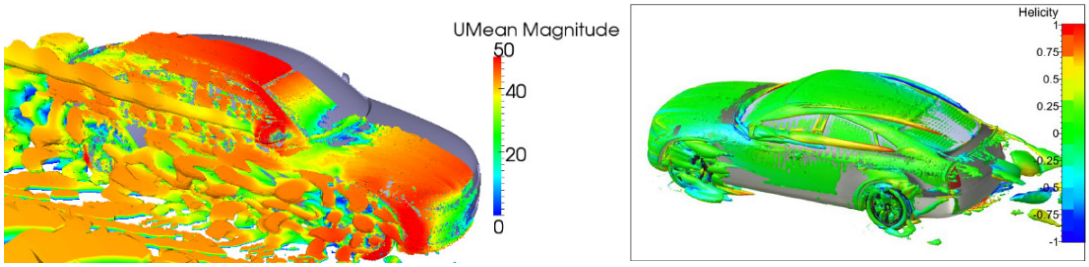

Fig. 10. Iso-surface of the second invariant (Q) based on mean velocity magnitude. Current study (Left), Study by Guilmineau (Right) [2]

Figure 11 shows the streamlines at the symmetry of the DrivAer Fastback model that is constructed using the time-averaged velocity flow field. The flow remains attached at the rear window and two counter rotating vortices are observed at the wake of the model. This result also very similar to the study done by Guilmineau [2].

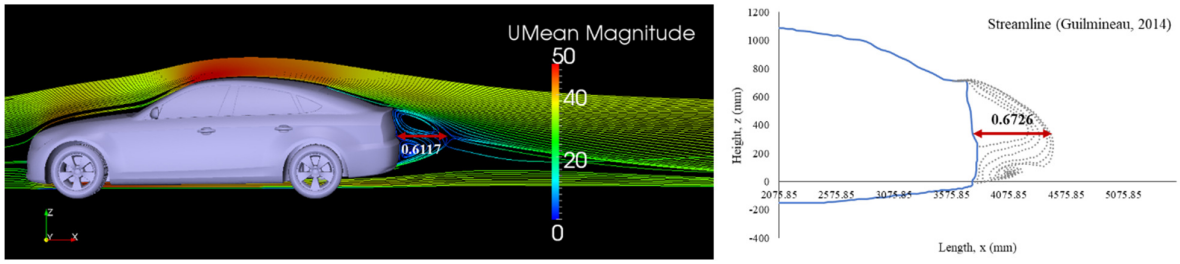

Fig. 11. Streamline at the symmetry of the model. Current study (Top), Study by Guilmineau (Bottom) [2]

By comparing the wake length for the DrivAer Fastback model with Guilmineau [2], it can be seen that the wake length produced by current study is only about 9% shorter than the study done by Guilmineau. The pressure coefficient results obtained from the fine grid is also compared with the experimental and numerical data by Guilmineau [2] study. The dimensionless pressure coefficient is defined as;

$$c_p = \frac{p - p_\infty}{0.5 \rho u_\infty^2} \tag{19}$$

where p is the local static pressure and p_∞ is the free stream static pressure.

The pressure coefficient distribution on top and bottom of the symmetry plane of the DrivAer Fastback model are shown in Figure 12 and Figure 13, respectively. Generally, the pressure coefficient for current study has shown a good agreement as the experimental data provided by Guilmineau [2]. Meanwhile, there is only some small discrepancies observed when compared with the numerical data.

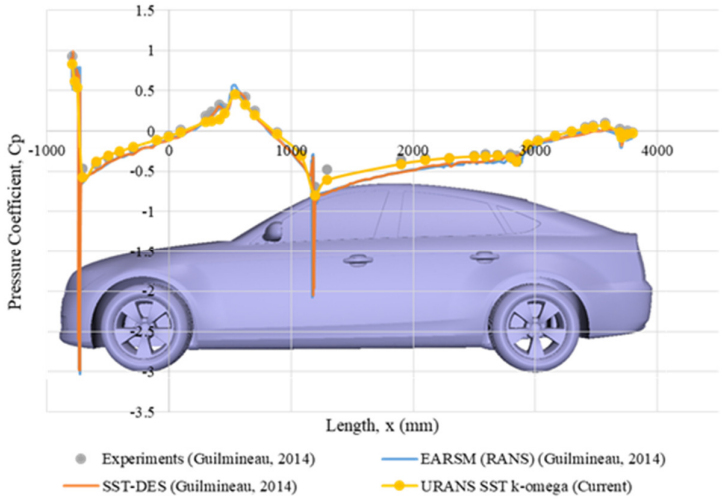

Fig. 12. Pressure coefficient (Cp) distribution on top of DrivAer Fastback model at the symmetry plane

Figure 12 compares the pressure coefficient along the top surface of the model between the current study and previous experimental and numerical studies by Guilmineau [2]. Current study is able to reproduce the same pressure distribution as the previous experimental study. A stagnation point is observed at the beginning of the measurement points where a sudden drop in pressure is observed. This is due to the flow separation occurred in front of the model [5]. The flow then recover at which the pressure slowly increased with distance downstream. At the junction between the hood and windshield, a peak in pressure is observed as the flow tends to separate before the pressure slowly decreasing over the windshield. This is a point where the favourable pressure gradient starts to occur. In current study, speedy pressure recovery behaviour is observed in front of the roof junction and it continues to increase gradually further downstream. The pressure then rises slowly at the rear window and a sudden decrease in pressure is found at the end of the model that shows that there is a flow detachment created.

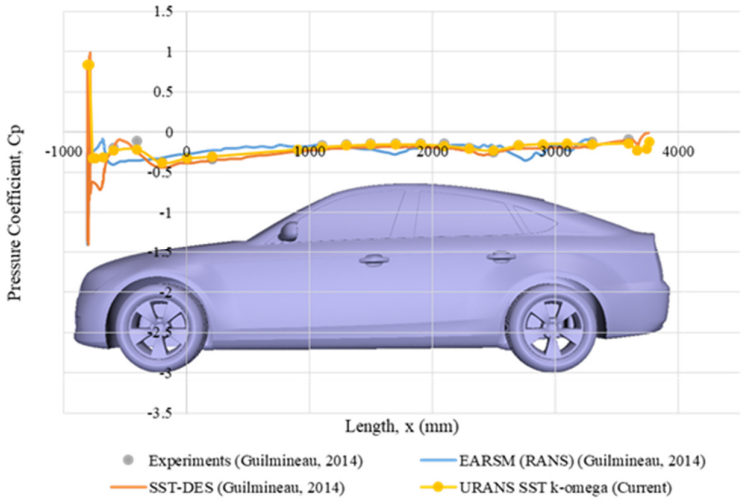

Fig. 13. Pressure coefficient (Cp) distribution below of DrivAer Fastback model at the symmetry plane

A good agreement with the previous experimental and numerical studies is also observed for the pressure distribution along the bottom surface of the model where the pressure coefficient gives a negative value starting from the beginning of the front wheels. The current study gives a better similarity with the previous experimental results. Based on the previous numerical study [2], small differences observed in front of the model is due to the different meshes used.

4. Conclusions

The grid convergence of flow around a realistic generic model, DrivAer has been numerically analysed that is based on a systematic assessment of computation grid refinement through the Grid Convergence Index (GCI) and Richardson extrapolation calculation. Based on the analysis performed, the calculated value of GCI gradually reduced as the grid system is refined. Results from the fine grid for both parameter have shown that the grid is appropriate to be used for further analysis. This is due to the GCI value of fine grid is less than 7%. Additionally, the drag coefficient obtained in the current study for the fine grid shows a good agreement with the previous studies with only less than 6% difference. Flow visualisation results also have captured the similar characteristics as the previous experimental study. The results of pressure coefficient on top and at bottom of the DrivAer Fastback

model also have shown a similar pattern as the previous experimental results. Therefore, it can be concluded that the results of current study are practicable for further studies. Additionally, the study shows that by properly refining the grid systematically, the use of excessive number of grid can be prevented through a systematic mesh refining using Richardson extrapolation and Grid Convergence Index (GCI) method. Small number of grid usage reduces the simulation time and reduces the computational costs at once that are preferred by the industries.

Acknowledgement
This research is financially supported by the Ministry of Higher Education (MOHE) Malaysia under the Research University Grant (RUG) project of Universiti Teknologi Malaysia (Vot No. R.K130000.7843.4F712), High Performance Computer (HPC) Universiti Teknologi Malaysia for the use of their supercomputer facilities and also Malaysia-Japan International Institute of Technology (MJIIT) Incentive.

References

[1] A. I. Heft, T. Indinger, and N. A. Adams, "Experimental and Numerical Investigation of the DrivAer Model," *Proc. ASME 2012 Fluids Eng. Summer Meet.*, vol. July 8-12, no. FEDSM2012-72272, pp. 1–11, 2012.
[2] E. Guilmineau, "Numerical Simulations of Flow around a Realistic Generic Car Model," *SAE Int. J. Passeng. Cars - Mech. Syst.*, vol. 7, no. 2, pp. 2014-01–0607, 2014.
[3] G. Shinde, A. Joshi, and N. Kishor, "Numerical Investigations of the DrivAer Car Model using Opensource CFD Solver OpenFOAM Numerical Investigations of the DrivAer Car Model using Opensource CFD Solver OpenFOAM Abstract," in *Tata Consultancy Services, Pune, India*, 2016, no. October 2013, pp. 0–12.
[4] N. Ashton, A. West, S. Lardeau, and A. Revell, "Assessment of RANS and DES methods for realistic automotive models," *Comput. Fluids*, vol. 128, pp. 1–15, 2016.
[5] D. E. Aljure, J. Calafell, A. Baez, and A. Oliva, "Flow over a realistic car model: Wall modeled large eddy simulations assessment and unsteady effects," *J. Wind Eng. Ind. Aerodyn.*, vol. 174, no. December 2017, pp. 225–240, 2018.
[6] S. R. Ahmed, G. Ramm, and G. Faltin, "Some Salient Features of The Time-Averaged Ground Vehicle Wake," *SAE Tech. Pap. Ser.*, 1984.
[7] N. H. Shaharuddin, M. S. M. Ali, S. Mansor, S. Muhamad, S. A. Zaki, and M. Usman, "Flow simulations of generic vehicle model SAE type 4 and DrivAer Fastback using OpenFOAM," *J. Adv. Res. Fluid Mech. Therm. Sci.*, vol. 37, no. 1, pp. 18–31, 2017.
[8] A. I. Heft, T. Indinger, and N. A. Adams, "Introduction of a New Realistic Generic Car Model for Aerodynamic Investigations," 2012.
[9] I. Celik, U. Ghia, P. J. Roache, and C. Freitas, "Procedure for Estimation and Reporting of Uncertainty Due to Discretization in CFD Applications," *J. Fluids Eng.*, vol. 130, no. 7, p. 78001, 2008.
[10] H. Jasak, "Error Analysis and Estimation for the Finite Volume Method with Applications to Fluid Flows," 1996.
[11] L. F. Richardson and J. A. Gaunt, "The Deferred Approache to the Limit. Part I. Single Lattice. Part II. Interpenetrating Lattices," *Philos. Trans. R. Soc. London. Ser. A, Contain. Pap. a Math. or Phys. Character*, vol. 226, pp. 299–361, 1927.
[12] P. J. Roache, "Perspective: A Method for Uniform Reporting of Grid Refinement Studies," *J. Fluids Eng.*, vol. 116, pp. 405–413, 1994.
[13] M. S. M. Ali, C. J. Doolan, and V. Wheatley, "Grid Convergence Study for a Two-Dimensional Simulation of Flow Around a Square Cylinder At a Low Reynolds Number," *Seventh Int. Conf. CFD Miner. Process Ind. CSIRO*, no. December, pp. 1–6, 2009.
[14] I. A. Ishak, M. S. M. Ali, and S. A. Z. Shaikh Salim, "Mesh size refining for a simulation of flow around a generic train model," *Wind Struct. An Int. J.*, vol. 24, no. 3, pp. 223–247, 2017.
[15] N. M. Maruai, M. S. M. Ali, M. H. Ismail, and S. A. Zaki, "Flow-induced vibration of a square cylinder and downstream flat plate associated with micro-scale energy harvester," *J. Wind Eng. Ind. Aerodyn.*, vol. 175, pp. 264–282, 2018.
[16] A. Cogotti. "Parametric Study on the Ground Effect of a Simplified Car Model," *SAE Paper*, 1998.
[17] F. Stern, R. V. Wilson, H. W. Coleman, and E. G. Paterson, "Comprehensive approach to verification and validation of CFD simulations part 1: Methodology and procedures," *Journal of Fluids Engineering,* 123(4), 793-802, 2001.
[18] D. C. Wilcox, "Turbulence Modelling for CFD, 3rd Ed., DCW Industries, Inc," 2006.